International Journal of Nanomedicine

Dovepress

open access to scientific and medical research

Open Access Full Text Article

ORIGINAL RESEARCH

Concurrent Tissue Engineering for Wound Healing in Diabetic Rats Utilizing Dual Actions of Green Synthesized CuO NPs Prepared from Two Plants Grown in Egypt

Noha Khalifa Abo Aasy[1], Sarah A El-Lakany[1], Perusi M Masanga[2], Elbadawy A Kamoun[3,4], Shahira H EL-Moslamy[5], Marwa Abu-Serie[6], Rania G Aly[7], Nazik A Elgindy[1]

[1]Department of Industrial Pharmacy, Faculty of Pharmacy, Alexandria University, Alexandria, Egypt; [2]St John's University of Tanzania, Dodoma, Tanzania; [3]Polymeric Materials Research Department, Advanced Technology and New Materials Research Institute (ATNMRI), City of Scientific Research and Technological Applications (SRTA-City), New Borg El-Arab City, Egypt; [4]Nanotechnology Research Center (NTRC), The British University in Egypt (BUE), El-Sherouk City, Cairo, 11837, Egypt; [5]Bioprocess Development Department (BID), Genetic Engineering and Biotechnology Research Institute (GEBRI), City of Scientific Research and Technological Applications (SRTA-City), New Borg El-Arab City, Alexandria, 21934, Egypt; [6]Medical Biotechnology Department (MBD), Genetic Engineering and Biotechnology Research Institute (GEBRI), City of Scientific Research and Technological Applications (SRTA-city), New Borg El-Arab City, Alexandria, 21934, Egypt; [7]Department of Surgical Pathology, Faculty of Medicine, Alexandria University, Alexandria, Egypt

Correspondence: Sarah A El-Lakany, Department of Industrial Pharmacy Faculty of Pharmacy, Alexandria University, 1 El Khartoum Square, PO Box 21521, Alexandria, Egypt, Tel +201002828663, Fax +203 4871668, Email sarah.ellakany@alexu.edu.eg; sarah.abdalla89@gmail.com

Purpose: Diabetes mellitus is among the disrupting factors of orchestrated events in wound healing. This necessitates the urge for tailored medications, which are continually offered by nano-sized materials. Herein, we present greenly synthesized copper oxide nanoparticles (CuO NPs), obtained from either *Punica granatum L.* (PG) or *Pisidium guajava L.* (GV) extract, to function as potent bactericidal and fungicidal materials that promote regeneration and healing of the targeted diabetic wounded tissues.

Methods: PG or GV plant extracts were compared as source of reducing agents for CuO NPs synthesis process. The yield and photocatalytic degradation potential were compared. NPs obtained from the superior extract, PG, were characterized using particles size, zeta potential, XRD, TEM, SEM, and EDX. The antimicrobial effects were evaluated on multidrug-resistant human pathogens and then the percentage biofilm inhibitory concentration was determined. The cytotoxicity and wound scratch study were conducted on a normal human skin cell line. In-vivo wound healing activity in diabetic rats was assessed along with histopathological and immunohistochemical examination of CD45 and α-SMA.

Results: The greenly synthesized CuO NPs are spherical in shape having a diameter of 233nm. CuO NPs (250µg/mL) acted as promising biocontrol agent against a variety of multidrug-resistant human pathogens. They significantly exhibited 29.460±0.811% healing of the scratched wound compared to only 2.001±0.155% for the control. Wound healing experiments revealed the safety of a low CuO NPs concentration in a diabetic animal model as well as on human normal skin fibroblast cell line. The treated group with a dose of 2mg/cm^2 showed superior results with a WC50 value of 7.2 days, and 92% wound contraction after 13-days. Immunohistochemical investigation of the same group demonstrated well-established fibrous tissue (5.7±3.7/HPF), and an amplified granulation tissue of recently developed blood vessels (70±1.5/HPF).

Conclusion: Green synthesized CuO NPs could overcome drug resistance and promote wound healing process effectively.

Keywords: plant extraction, metal ion, cell compatibility, wound contraction, biofilm inhibitory concentration

Introduction

The optimal skin wound healing process involves an established coordination between both biological and molecular events, within a proper time frame, during the well-known healing stages, namely inflammatory, proliferative, and remodeling. Unfortunately, the disruption of such orchestrated events results in an impaired healing process. One major cause is Diabetes

Received: 30 November 2022
Accepted: 4 April 2023
Published: 10 April 2023

mellitus, where diabetic patients are more vulnerable to delayed healing with the accompanying health complications. In fact, diabetes mellitus is a metabolic disorder that may result in severe neurodegeneration, where diabetics suffer from low nitric oxide levels. Nitric oxide is a key moiety that can interact with many intracellular targets to trigger an array of signal transduction pathways, resulting in stimulatory or inhibitory output signals.[1–3]

Although xenografts, allografts, and autografts are the biomedical approaches of choice, their employment is highly retarded due to their use-related risks including poor healing process, high antigenicity, infection hazards, and donor site restrictions.[4] This necessitates the urge for tailored medications with appealing characteristics, which are continually offered by nano-sized materials.

Copper oxide nanoparticles (CuO NPs), nano-crystalline materials made of copper metal cations along with oxide anions, are currently of one of the most prominent metal oxide NPs. On one hand, these NPs exhibit appealing properties of metal ions including their hydrophobicity, porosity, and surface charge.[5] On the other hand, compared to other metal oxides such as oxides of silver and gold, CuO is more cost-effective, readily available, less toxic, vastly stable, and simply manufactured.[6] Moreover, the copper element itself is a trace element compulsory for many vital functions as a cofactor for various enzymes involved in well-being of the immune system. The design of the CuO in the nano-range boosts the products' physical properties where the large surface-to-volume ratio indeed promotes the antibacterial, antioxidant, antifungal, wound healing, and anticancer applications through the interaction of the NPs with the biological barriers and their entry into the living cell.[7] Most importantly, CuO NPs usage overcomes the rapid development of antibiotic drug resistance to bacterial strains, which is considered among the top 10 reasons for mortality and amputation in diabetic patients.[8]

When synthesizing CuO NPs, the hazards of the synthesis methods are a major concern. For instance, in traditional chemical preparation methods, inorganic chemicals including sodium or potassium borohydride are used to reduce metal to metal oxide, exposing the surrounding environment to toxic by-product contamination.[9] Although the physical synthesis method offers the complete absence of solvent contamination, high and continuous energy consumption is needed to prevent any fluctuation in the parameters of this method. Highly complex instrumentation is also involved in the physical method.[10] Such restrictions limit the use of chemical or physical approaches to synthesize metal oxide NPs.

Ecofriendly biological synthesis methods are gaining more attention because of their alluring properties, compared to other methods, making them interesting candidates to fabricate metal oxide NPs.[10] In brief, these methods involve the building up of atom to atoms, molecule to molecules, and cluster to clusters that result in the formation of NPs. The reduction and stabilizing activities resembling that in chemical methods occur via natural phytochemicals eliminating the usage of toxic chemicals with the ease of scaling up the process. These plant-derived phytochemicals behave as safe metal salt-reducing agents to produce metal oxide NPs.[11]

The formulation of CuO NPs involves two steps: extraction of phytochemicals from plant parts and then plant extract and copper salt were utilized in the development of CuO NPs. Scientists are increasingly using plants for the synthesis of NPs, due to their expected safety as the use or production of any toxic substance is absent. Previously, eco-friendly CuO NPs were successfully synthesized by mixing various copper salts, as a source of precursor metal, with different plants such as *Tamarix gallica*,[12] *Allium sativum*,[13] *Momordica charantia*,[6] *Ixiro coccinea*,[14] *Syzygium alternifolium wal*,[15] *Madhuca longifolia*,[16] *Achillea millefolium*,[17] *Psidium guajava*,[11] *Ficus religiosa,*[8] and *Bougain villea*[18] extracts.

In the current study, we chose to compare the effect of prepared green synthesized CuO NPs obtained from the extracts of two plants grown in Egypt: peels of *Punica granatum L*. (PG), Family *Lythraceae*, or leaves of *Psidium guajava L*. (GV), Family *Myrtle*, in promoting the healing of diabetic wounds in rats. The two plants show promising phytochemical composition that can be used to produce stabilized CuO NPs. Moreover, both extracts, enriched with flavonoids, tannins, and glycosides, exhibit pharmacological actions such as anti-inflammatory, wound healing, anti-bacterial, antioxidant, and anticancer potentials.[13,17–20] CuO NPs are anticipated to function as potent bactericidal as well as fungicidal materials with an ability to promote healing of the targeted wounded tissues and aid in its regeneration, where the mechanism underlying such activities include generation of enzyme disruption, inhibition of DNA replication, solubilization of NPs, protein denaturation, and acting as a cofactor for vital enzymes synthesis.[10] Optimization techniques for preparation, yield, and time and stir type will be studied. The optimized formulae were tested for their possible application in tissue regeneration and wound healing, especially for diabetic wounds.

Materials and Methods

Materials

Bacterial Strains, Plant Material, and Chemicals

Gram-negative bacterial cells (*Salmonella paratyphi* ATCC 9150, *Shigella spp*. ATCC 11126, *Pseudomonas aeruginosa* ATCC 27853, and *Escherichia coli* ATCC 10536), Gram-positive bacterial cells (*Streptococcus spp*. ATCC 49619, *Staphylococcus epidermidis* ATCC 12228, and *Staphylococcus aureus* ATCC 6538) as well as fungal cells (*Candida krusei* ATCC 6258, *Saccharomyces cerevisiae* ATCC 9763, and *Candida albicans* ATCC 10231) were provided by the Bioprocess Development Department, Genetic Engineering and Biotechnology Research Institute, City of Scientific Research and Technological Applications, Egypt. Copper sulfate ($CuSO_4.5H_2O$) was obtained from Alpha Xhemika, India. Both plants were supplied from the local Egyptian market, *Punica granatum L*. (PG), Family *Lythraceae* peels powder was purchased from El-Zaafarany Co. (Batch number6287000000313), while *Psidium guajava L*. (GV), Family *Myrtle* leaves powder were purchased from ISIS Co. (Batch number 6227000471487). Poloxamer 407 (PLX), sterilized Mueller Hinton broth, and 3-(4,5-dimethylthiazol 2-yl) 2,5-diphenyl tetrazolium bromide (MTT) were purchased from Sigma Aldrich Chemie, ST. Louis USA. Normal human skin fibroblast HBF4 cell line was purchased from the American Type Culture Collection (ATCC). Sterile-filtered Dulbecco's modified Eagle's medium (DMEM) high glucose with L-glutamine was purchased from BioWhittaker (Lonza, Belgium). CD45 (Ready to use primary antibody, mouse anti-human, monoclonal antibody, P0042) and α-SMA (Ready to use primary antibody, mouse anti-human, monoclonal antibody, P0943) were purchased from Leica Biosystems, USA.; Leica Biosystems, USA. Other reagents and chemicals were used in an analytical grade.

Green Synthesis of CuO NPs

Preparation of Extracts of PG Peels and GV Leaves

To prepare plant extract, 10 g of obtained plant powder was weighed separately, mixed with 100 mL of distilled water, and left on a magnetic stirrer for 10 min at 55°C. After cooling, each mixture was filtered to be used in CuO NPs preparation.

Formulation and Optimization of CuO NPs

3 mM of copper sulfate ($CusO_4.5H_2O$) salt was dissolved in 100 mL of distilled water. Then, 2 g of poloxamer 407 (PLX) was added to the salt solution and was kept in the fridge at ~ (2–8°C), till all PLX was completely dissolved. A volume of 10 mL of the formed salt solution was added to 90 mL of either PG or GV extract and mixed under magnetic stirring (Ika Labortechnik, Germany) for 5 min at room temperature. The light blue salt solution was instantaneously changed to green, and then it gradually transformed to a brown color, indicating CuO NPs formation. The mixture was subjected to centrifugation (Sigma Laboratory Refrigerated Centrifuge, Model 3K-30, Germany) at 8000 rpm for 10 min, filtration, and washing with aqueous ethanolic solution (50% v/v ethanol). The residue was air-dried at room temperature, then weighed to determine the obtained yield.

Various process variables were screened for maximum yield and optimum particle size (PS). First, different concentrations of $CuSO_4.5H_2O$ salt ranging from 3 mM to 20 mM were studied, where a selected salt concentration of 15 mM was used for further investigation. Afterwards, the duration of magnetic mixing varied between 5 and 180 min. Finally, different mixing equipment including a magnetic stirrer, homogenizer, and sonicator were investigated.

Physicochemical Characterizations of CuO NPs

CuO NPs formation was verified using T80UV–visible double beam spectrophotometer (PG Instruments Ltd., UK). The optical absorbance of the NPs was measured in the wavelength range of 200–600 nm.[6]

The chemical composition of CuO NPs was analyzed using FT-IR (IR, 8400s Shimadzu, Japan) following the formation of the KBr disc. The IR fingerprints were recorded within the wavenumber region of 4000–400 cm^{-1}.[21]

Both PG and GV-mediated CuO NPs size, shape, and size distribution were characterized by using the transmission electron microscope (TEM, JEM-100 CX, JEOL, Japan) and scanning electron microscope (SEM, Joel GSM-6610LV, Japan). For TEM, a sample was performed by placing the particles on a copper grid. Eventually, digital micrograph and soft imaging viewer software were used. For SEM, NPs were coated with a thin gold layer using a sputter coater before imaging at an operating voltage of 5 kV under vacuum.[14]

Photocatalytic degradation activity of PG and GV synthesized CuO NPs was measured. In brief, 10^{-4} M of Methyl blue (MB) or Methyl orange (MO) dye solutions were mixed with 1mL of the aqueous solution of ascorbic acid (10^{-2} M) and PG or GV synthesized CuO NPs (10^{-4} M) in a ratio of 1:1:1, respectively, and their absorption wavelengths were scanned over the wavelength range 200–700 nm. Eventually, the spectra were compared to the spectra of each dye solution alone and aqueous solutions of dye and ascorbic acid using UV/Vis spectrophotometer.[22]

The average PS, polydispersity index (PDI), and zeta potential (ZP) of CuO NPs were recorded using a Zetasizer instrument (Malvern Instrument NanoZS, UK) applying dynamic light scattering (DLS) technique. The samples were appropriately diluted via distilled grade water, before each assessment, to circumvent the multi-scattering phenomena resulting from highly concentrated solutions. While for ZP measurement, a disposable folded capillary cell was loaded with 1 mL of each diluted solution. Measurements were performed in triplicate at 25 ± 0.5°C and data were recorded as mean ± SD.[23]

In addition, the X-ray diffraction pattern of CuO NPs (prepared using PG) was obtained using a powder X-ray diffractometer (XRD, X`Pert PRO MPD diffractometer, Philips Analytical, The Netherlands) with Cu Ka radiations (k = 1.54060 nm) in 2 h range to guarantee CuO NPs purity.

Energy-dispersive X-ray detector (EDX, LEO 435VP, Carl Zeiss™ AG, Oberkochen, Germany) at 15 kV was used for the determination of the elemental composition analysis of CuO NPs (prepared using PG).[24]

In-vitro Antimicrobial Efficacy of CuO NPs

In the investigations that follows, the minimal inhibitory concentration (MIC), minimal fungicidal concentration (MFC), minimal bactericidal concentration (MBC), and minimal biofilm inhibitory concentration (MBIC) were estimated after surveying the antimicrobial efficacy of CuO NPs dosages using the "well diffusion" and "micro-dilution" assays.

Screening of Antimicrobial Activities for CuO NPs

Cryopreserved pathogen cultures were revived by inoculating them in a rich Luria-Bertani (LB) broth medium. To obtain the mentioned broth medium, 10 g of tryptone, 10 g of sodium chloride, and 5 g of yeast extract were dissolved in 1L of distilled water. These cultures were incubated for 72 h at 37°C and 200 rpm. The inoculums of these grown pathogens were streaked separately on LB agar plates and incubated statically for 18 h at 37°C. Then, the potential antimicrobial efficacy of various CuO NP doses (50, 100, 150, 200, and 250 µg/mL) was examined using the well diffusion method.[25–27] Aliquots of these pre-cultures were re-suspended in sterile saline (0.8% sodium chloride), then swabbed over the solid LB plates' surface (90 mm). Wells were then cut using metal cork borers' 5 mm diameter and loaded with 100 µL of various tested CuO NPs dosages. Subsequently, these plates were incubated for 48 h at 30°C for fungal cells and 37°C for bacterial cells. The average values of the generated inhibitory zones were then quantitatively and statistically assessed. Subsequently, the antimicrobial effectiveness of CuO NPs was also tested using the broth micro-dilution method.[28] In brief, utilising the 0.5 McFarland turbidity standards, overnight culture strains were generated using LB broth. The same tested CuO NPs dosages (50, 100, 150, 200, and 250 µg/mL), excluding controls, were then administered to the tested cultures (cultures without CuO NPs). All these cultures were incubated at 200 rpm and 37°C for one night. Aliquots of each culture and its controls were periodically sampled to determine the quantitative measurements of the turbidity's absorbance at 600 nm. Each experiment was run three times to minimize errors.

Determination of Biofilm Inhibitory Concentration

Colony count was used to evaluate the viability of biofilm cells. Briefly, each of the assessed human pathogens was individually inoculated in LB broth medium (2×10^5 CFU/mL). Different doses of CuO NPs (50, 100, 150, 200, and 250 µg/mL) were added at that time under aseptic conditions, except for the controls, which were not treated with CuO NPs. These cultures were then incubated at 37°C and 200 rpm for 24 h. The generated biofilm was then centrifuged (10,000 rpm for 15 min at 4°C) before being rinsed with 200 µL phosphate-buffered saline. After washing, the NPs were re-suspended by adding 100µL of PBS, and then pipetted vigorously. Serial dilutions of these suspended biofilms were prepared and swabbed over to LB agar medium and incubated for 48 h. Finally, the percentage of biofilm inhibitory concentration was calculated by counting the generated colony-forming units per millilitre (CFU/mL).[25,29,30] Three replicates of each experiment were performed twice.

Determination of MIC, MBC, and MFC

The dose-dependent method was applied using varying concentrations of CuO NPs (50–600 µg/mL).[31] Microbial growth was monitored visually in LB broth culture at 37°C for 24 h. Then the microbial growth was visually evaluated by assessing the turbidity of the culture. Finally, the micro-biostatic effect was determined by detecting the lowest CuO NPs concentration at which turbidity is undetectable Viable microbial cells were counted to determine MBC and MFC. In brief, 100 µL of these cultures were spread out on agar LB plates and incubated at 37°C for 24 h to examine only the survival of microbial cells.[32]

Ex-Vivo Studies

Determination of Cytotoxicity of CuO NPs on Normal Skin Cells

The cytotoxicity of CuO NPs was evaluated on a normal human skin fibroblast HBF4 cell line using 3-(4,5-dimethylthiazol 2-yl) 2,5-diphenyl tetrazolium bromide (MTT) assay as previously described by Krishnan, B.R. et al[33] The effective doses (IC_{50} and EC_{100}) of the CuO NPs at which 50% and 100% cell viability, respectively, were estimated by GraphPad Instat software.

Wound Scratch Healing Assay

Normal skin cells (HBF4) were cultivated in DMEM medium (10% fetal bovine serum). The cells were seeded at a concentration of 3×10^5 cells per well in a culture plate. After 24 h incubation, around 90% confluent cell monolayer was obtained. With the aid of a sterile pipette tip, a small area was scratched. A sample of CuO NPs (1 mg) was washed and then placed with the cells for 24 h in a 5% CO_2 incubator. The scratched area was imaged by a digital camera attached to the phase-contrast inverted microscope with a digital image analysis system (Analysis 3.1 Soft Imaging System SIS). The percentage of wound closure was estimated by image j software.[23,34]

Bio-Evaluation Tests

In-Vivo Wound Assessment

Animals

Twenty-one mature male albino rats (average 200–250 g) were enrolled in the assessment. The animals were kept in standard metal cages at 21±1°C, relative humidity (65%) with a 10 h light/14 h dark cycle. Prior to the experiment, rats were allowed to accommodate for 2 weeks. The animals lived on standard chow and water ad libitum for the study period at the animal house of the Faculty of Medicine, Alexandria, Egypt. Approval of ethical committee was obtained, and animals were handled according to the ethical guidelines of Alexandria University (Au: 06/2022/9/5/1/126). Furthermore, animal experiments followed the ARRIVE guidelines and the UK Animals (Scientific Procedures) Act, 1986, and associated guidelines, EU Directive 2010/63/EU for animal experiments.

Induction of Excision Diabetic Wound

To induce diabetes in the animals, diethyl ether was first administered, as an anesthetic to 21 male rats. Afterwards, the rats were injected with 60 mg/kg streptozotocin intraperitonially (I.P. injection). Then, the blood-glucose level was measured by Accu-Chek Active (Roche Diagnostics GmbH, Germany). A rat with glucose levels in the blood exceeding 300 mg dL^{-1} was considered a diabetic animal model. After 14 days, rats were hypnotized by (3% w/v) pentobarbital sodium solution (1mg/kg, I.P.) and the skin of each rat dorsum was shaved cautiously.[5,35] Subsequently, the skin was sterilized by both: cetrimide-chlorhexidine (1:30) solution and ethanol (70%), and 1 cm^2 full-thickness rounded-skin wounds were developed on the dorsal area of each male rat.[34,36]

The wounded rats were divided into three groups: untreated positive controls, 10 mg/cm^2 CuO NPs powder (Gp1)-treated group and 2 mg/cm^2 CuO NPs powder (Gp2)-treated group. On days 0, 3, 7, and 10, CuO NPs powder (2 or 10 mg/cm^2) was topically applied to the wound zones of treated groups and shielded with a porous 3M Micropore TM adhesive tape. On days 0, 3, 7, 10, and 13, pictures of the wound regions were taken, and the wound closure percentage was determined as a % reduction in wound area compared to the original area at zero time as well as the wound half closure time (WC_{50}) were calculated. On day 13 consequent to the wounding, rats were sacrificed for histological and immunohistochemical examination of the expression of CD45 and α-SMA antibodies.

Histopathological Examination

The histological examination of wounded sections of the skin was performed after their staining with hematoxylin and eosin (H&E), using a light microscope (Leica, Germany). The mean value of the % of the formed granulation and fibrous tissues, as well as the epidermal thickness, was quantified via ImageJ, v1.53 (Maryland, USA). A scoring system of the hair follicles, skin appendages, and sebaceous glands was established where no skin appendages; 1, few <5/wound area; 2 and ≥5/wound area; 3. Furthermore, Masson Trichrome staining (MTS) was performed on the sections. Image color deconvolution v1.53 (Maryland, USA) was utilized to quantify the percentage area of fibrosis in each specimen.

Immunohistochemical (IHC) Staining and Interpretation

The Avidin-Biotin-Peroxidase method was performed to study the IHC changes in the wounded sections. α-SMA (Ready to use primary antibody, mouse anti-human, monoclonal antibody, P0943; Leica Biosystems, USA) and CD45 (Ready to use primary antibody, mouse anti-human, monoclonal antibody, P0042; Leica Biosystems, USA) were employed, in the current study, to stain the lymphocytes, blood vessels, and myofibroblasts, respectively. Antibodies were added to each section using the Bond-Max fully automated immunostainer (Leica Biosystems, USA). Positive control for each primary antibody using tonsil and leiomyoma and negative control (omitted primary antibody) were included in each run. The IHC quantification of α-SMA and CD45 was evaluated on each slide using quantitative-image analysis (Leica Microsystems, Switzerland).[5]

Statistical Analysis

All measurements were carried out at least in triplicate. Data are displayed as mean ± standard error of the mean (SEM). ANOVA and Tukey multiple comparisons tests were used to compare the results of each group statistically using Minitab 18 software (Minitab® 18.1, © 2017) using a one-way analysis variance (p-value ≤0.05).

Results and Discussion

Green Synthesis of CuO NPs

CuO NPs were successfully synthesized using either PG or GV extracts mixed with copper sulphate solution at room temperature, in accordance with previous studies.[30] PG or GV extracts were added to various concentrations of copper sulfate solution in a ratio of 1:9, a color change was clearly observed, where the original light blue varied to brown, then a black brownish color confirming the formation of CuO NPs, as shown in Figure 1i. The color change can be attributed to the reduction of precursor molecule copper, under the effect of various phytochemicals, into CuO NPs.[30] Plant extracts exhibit appealing active biomolecules including proteins, phenolics, terpenoids, flavones, polysaccharides, alkaloids, alcoholic compounds, amino acids, and enzymes. These biomolecules act as stabilizers, capping, and reducing agents, producing stable and shape-controlled NPs.[37]

As previously reported, the quantitative determination of an aqueous extract of GV leaves was found to contain high concentrations of phenol (8.0±0.5 mg/gm), flavonoids (5.34±0.36 mg/gm), tannin (4.80±0.30 mg/gm), and saponin (4.24 ±0.29 mg/gm). GC-MS analysis identified a total of 33 compounds and confirmed that GV encloses Bis(2-ethylhexyl) phthalate, Alpha-bisabolol, caryophyllene, 1, 2-benzenedicarboxylic acid, butyl, and nerolidol and germacrene as its main components.[38] Regarding PG, an Egyptian study was elaborated to determine the chief components of the aqueous extract of the Egyptian PG peels using GC-MS. Results revealed that the distinguished constituents are combinations of terpenes and related alcohols with a total of 13 compounds. Chief compounds were geranyl vinyl ether, benzaldehyde, benzoic acid, linalool, oleic acid, phenol, 2-methoxy-3 (2-propenyl), and eicosapentaenoic acid.[39]

Nagajyothi et al[19] reported CuO NPs probable formation mechanism where the unstable copper hydroxide molecule was formed after dissolving copper salt as a metal precursor in water, which in turn was reduced into CuO NPs by the extract incorporated biomolecules.

Optimization of the Green Synthesis of CuO NPs

The yield of the formed CuO NPs was adopted as a significant parameter in optimizing both formulation and process variables. It was observed that as the concentration of the copper salt was increased from 3 mM to 15 mM, the amount of the yield significantly increased (P<0.05) from 22.40 ± 2.05 to 54.0± 3.94 mg and from 16.63±1.40 to 25.22 ±076 mg, when PG and GV extracts were used, respectively (Table 1). Any further increase in copper sulphate concentration (above 15 mM and

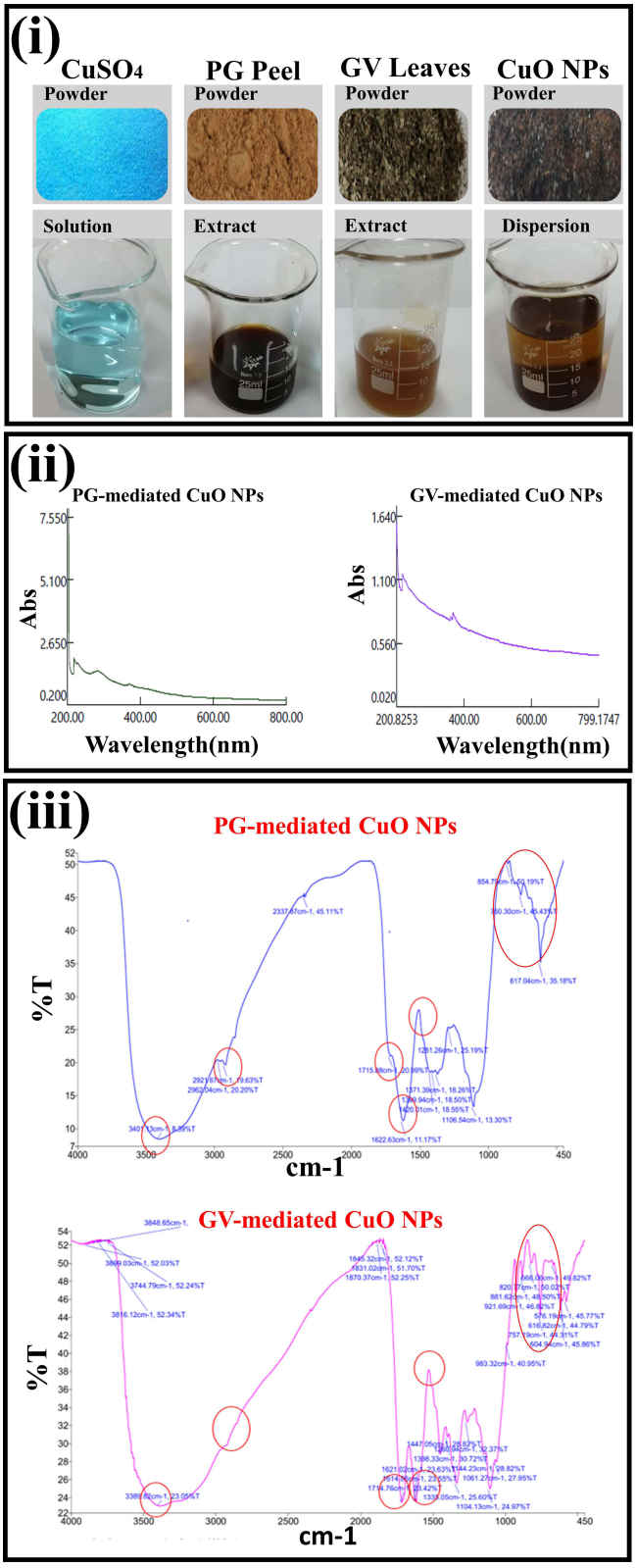

Figure 1 (**i**) Photographs of the powder form and its relevant aqueous preparation of hydrated $CuSO_4$, PG peel, GV leaves, and CuO NPs. (**ii**) UV-Visible spectra, and (**iii**) FTIR spectra of CuO NPs prepared from PG or GV extracts.

up to 20 mM) resulted in a clear reduction in the obtained yield. It is worth mentioning that different parts of the plants contain variable active biomolecule proportions and amounts, which would affect the obtained yields. A higher yield was obtained from the extract of the fruit peel of PG, compared to leaves of GV, which could be appertaining to the higher phytochemical composition of the more colorful PG plant extract and thus, its higher reducing ability.[9]

To maximize the obtained CuO NPs yield, different variables such as magnetic stirring, mixing times and techniques were examined. For PG extract, increasing magnetic stirring duration up to 180 min imparted a significant positive increase ($P<0.05$) in the amount of yield obtained as recorded in Table 1. On the contrary, upon using GV extract, the increase of mixing duration (up to 30 min) firstly boosted the amount of yield; however, further increasing the mixing time caused an insignificant change in the obtained NPs' yield.

This may be related to the kinetics of the reactants, which affects the amount of NPs yield, as the increase in yield may stop when all the reactants were consumed, and no further phytochemicals are present to reduce the copper sulfate into CuO NPs.[40] Although the introduction of more efficient mixing techniques such as homogenization and sonication for 5 min produced an insignificant increase in yield compared to magnetic stirring ($P>0.05$), these methods significantly shortened the duration of the preparation process, Table 1. On one hand, these techniques allowed the phytochemical to react or collide with the salt in a shorter duration of action, but on the other hand, the obtained PS was tremendously increased where huge aggregates were formed.[10] Based on the above findings, magnetic stirring for 30 min was chosen as the optimum condition for the preparation as it produced a satisfying yield amount, without any aggregate formation, and within the accepted time interval.

Table 1 The Influence of the Molar Concentrations of $CuSO_4.5H_20$, Magnetic Stirring Time (Min), and Mixing Technique on the Yield (Mg) of CuO NPs Prepared from *Punica Granatum* (PG) or *Psidium Guajava* (GV) Extract

Variables		Amount Yield in (mg±SD)	
		***Punica granatum* (PG)**	***Psidium guajava* (GV)**
Concentration of $CuSO_4.5H_20$ (mM)	**3**	22.40±2.05	16.63±1.40
	5	23.60±1.93	17.75±1.75
	7	24.53±1.77	18.54±2.00
	9	34.90±1.00	20.45±1.05
	11	36.90±0.65	22.85±0.55
	13	42.70±1.70	23.85±0.25
	15	54.00±3.94	25.22±0.76
	20	42.13±2.70	21.95±0.35
Magnetic stirring (min)*	**5**	54.00±3.94	25.22 ±0.76
	10	59.35±1.45	24.60 ±2.60
	30	61.05±1.15	23.85±1.85
	60	62.75±0.85	23.50±1.10
	180	74.65±2.35	24.75±1.35
Sonication (min)*	**5**	58.55±1.05	24.45±1.15
Homogenization (min)*	**5**	68.85±1.50	25.80±0.80

Note: *Using 15 mM of $CuSO_4.5H_2O$.

Characterization of CuO NPs

UV-VIS Spectroscopy

The UV–visible absorption spectra of CuO NPs prepared by PG or GV extracts displayed absorption peaks at λ ~ 264 and 380 nm, respectively, revealing the characteristic peaks of CuO, and confirming its formation, as shown in Figure 1ii.[6,41]

Fourier Transform Infrared Spectroscopy (FT-IR)

The spectra of CuO NPs prepared by the extracts of PG or GV plants revealed characteristic peaks at ν 3389 and 2926 cm^{-1}. These peaks indicate stretching of the O-H group of alcohol, phenol, N-H amines of amides, C-H stretching of alkanes, that may be present on the surface of CuO NPs, also C=O stretching at ν 1714 cm^{-1} of amide conjugation and C=C stretching at 1614.86 cm^{-1}. The wavelength at ν 1621 cm^{-1} is due to the stretching vibration of the C-OH bond from alcoholic to phenolic, while at ν 1447 cm^{-1} band is due to the C-N stretching of aliphatic and aromatic amine. Absorption peaks at ν 1335, 1260 and 1104 cm^{-1} may be due to the presence of stretching of COOH and amino groups, which leads to the capping and stabilization of CuO NPs. Three IR absorption peaks were observed to be in the range of ν 500–700 cm^{-1} due to the vibrational modes of Cu-O. Other major peaks were detected at ν 525, 580, and 675 cm^{-1} as shown in Figure 1iii. The same findings were reported in previous studies.[21,42]

TEM and SEM Investigation

TEM images revealed that CuO NPs showed spherical-shaped structures with the agglomeration of small particles forming a cluster shape. Distinct particles have small nanometric PS. The size of the particles calculated by the TEM ranged from 5 to 20 nm with an average particle diameter of 15 nm for CuO NPs prepared from PG extract and a larger size of 44 nm for those prepared by GV extract as displayed in Figure 2i. Aggregation of the particles caused a variation in size from the nano to micro range of the formed NPs.[14] SEM micrographs prepared by PG extract appeared as

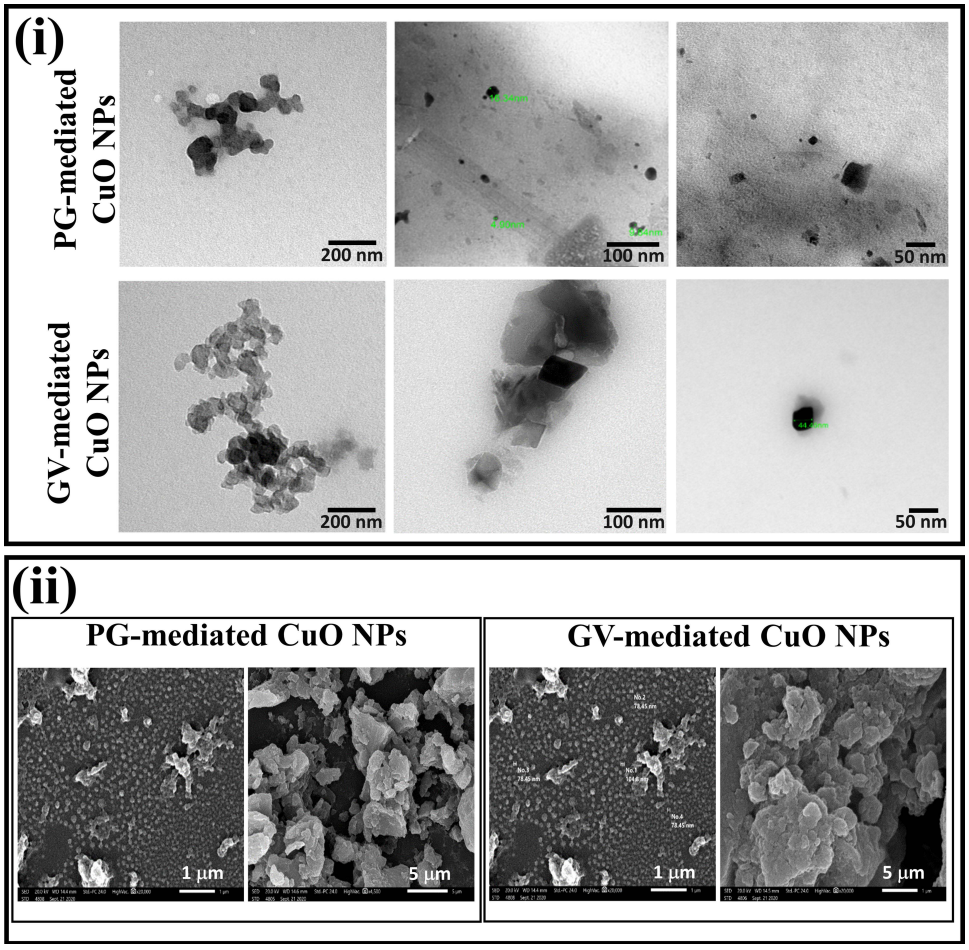

Figure 2 (**i**) TEM images and (**ii**) SEM images of CuO NPs prepared from PG or GV extracts showing different magnification powers.

spherical-like shaped particles with an average size range of 78−10^4 nm. NPs prepared by GV extract revealed a flake-like structure with high aggregation in the SEM micrographs (Figure 2ii).

Our findings agree with the results of Sathiyavimal et al[11] who reported that TEM and SEM micrographs of CuO NPs appeared as asymmetrical spherical particles in agglomerated platelets. Recent research investigated the green biosynthesis of CuO NPs from *Tamarix gallica* aqueous leaf extract where different sizes and shapes were obtained.[12] The authors indicated that using different biosynthesis methods resulted in the fabrication of diverse morphologies of CuO NPs. The authors stated that asymmetrically spherical-shaped CuO NPs in the nano range had better bactericidal activity.[7] In the current study, the results of TEM and SEM coincide with each other giving superiority to NPs prepared by PG extract.

Photocatalytic Degradation Activity

The photocatalytic activity of CuO NPs was elaborated using two photodegradable dyes MB and MO, where decreasing the peak intensities of the dyes is an indication of their degradation. The UV–VIS absorbance intensity peaks of MB and MO were observed at 660–665 nm, and 250–486 nm, respectively. The aqueous dyes' solutions absorbance intensity and peak wavelength were recorded in the presence of CuO NPs, under sunlight irradiation, where the degradation efficiency was compared to control dye solutions.

After 10 min of exposure, MB dye exhibited a degradation in color after occupation with CuO NPs (Figure 3i). CuO NPs prepared from PG showed a significant shift of MB peak from 664 nm to 624 nm with a 93.5% decrease in peak intensity (Figure 3ii). Notably, MO dye also exhibited a color degradation prior to engaging with the NPs for 10 min (Figure 3iii). MO peaks were also shifted from 250 nm to 242 nm with 75.5 peak degradation and from 486 nm to 367 with 55% decreased peak intensity, respectively. Regarding CuO NPs prepared from GV, MB peak showed a decreased intensity by 65% with no change in wavelength. The same was observed in MO peaks, where only 10% degradation was reported in the 250 nm peak (Figure 3iv). A possible explanation is that upon striking CuO NPs with sunlight, surface electron–hole pairs were produced. This led to the formation of hydroxyl radicals through a multi-electron reduction reaction. Thus, these produced active species reacted with aqueous dye molecules converting them into H_2O, CO_2, and decomposed mineral compounds.[43] In a previous study, the research team reported similar findings where acceptable photodegradation of MB treated with CuO, magnesium oxide, or zinc oxide NPs was observed.[22]

Based on the above results, CuO NPs prepared from GV extract were excluded from any further investigation where they showed a lower photocatalytic degradation potential and a lower obtained yield, compared to NPs obtained from PG extract.

Particle Size and Zeta Potential Measurement

DLS analysis showed that the average size of CuO NPs prepared from PG extract was 233 nm (Figure 3v), while ZP measurements exhibited a negative potential of about −15.8 mV as shown in Figure 3vi. Measurements of PS agreed with CuO NPs prepared from actinomycete extracts, which showed an average particle measurement of 198 nm, respectively. The negative ZP caused a strong repulsion force between the molecules, resulting in acceptable stability and quality of the CuO NPs.[44]

XRD and EDX Analysis

XRD pattern of PG extract mediated CuO NPs is shown in Figure 3vii. The diffraction patterns were observed to occur at 2θ = 9.6, 19, 22, 26, 30, 32.47, 35.49, 38.68, 48.65, 53.36, and 58.25. The spectrum resembles that of pure CuO, confirming the establishment of monoclinic structure of CuO in a single phase. The present experimental results agreed with the reported diffraction patterns of CuO NPs prepared by Padil and Černík.[45] In EDX analysis, NPs interaction caused an emission of X-rays that in turn provided information about the elemental composition of the sample and hence the purity of the formulation.[24] Results demonstrated strong signals in copper and oxygen, which further verified the formation of CuO NPs (Figure 3viii). The experiment reveals the good purity of CuO NPs as its elemental composition involves these two elements only.[11]

In-Vitro Antimicrobial Efficacy of CuO NPs

The agar diffusion assessment, which was required to accurately determine CuO NP's antimicrobial activities, showed significantly different inhibition zones against all tested pathogens, except for the tested fungal cells, which did not show

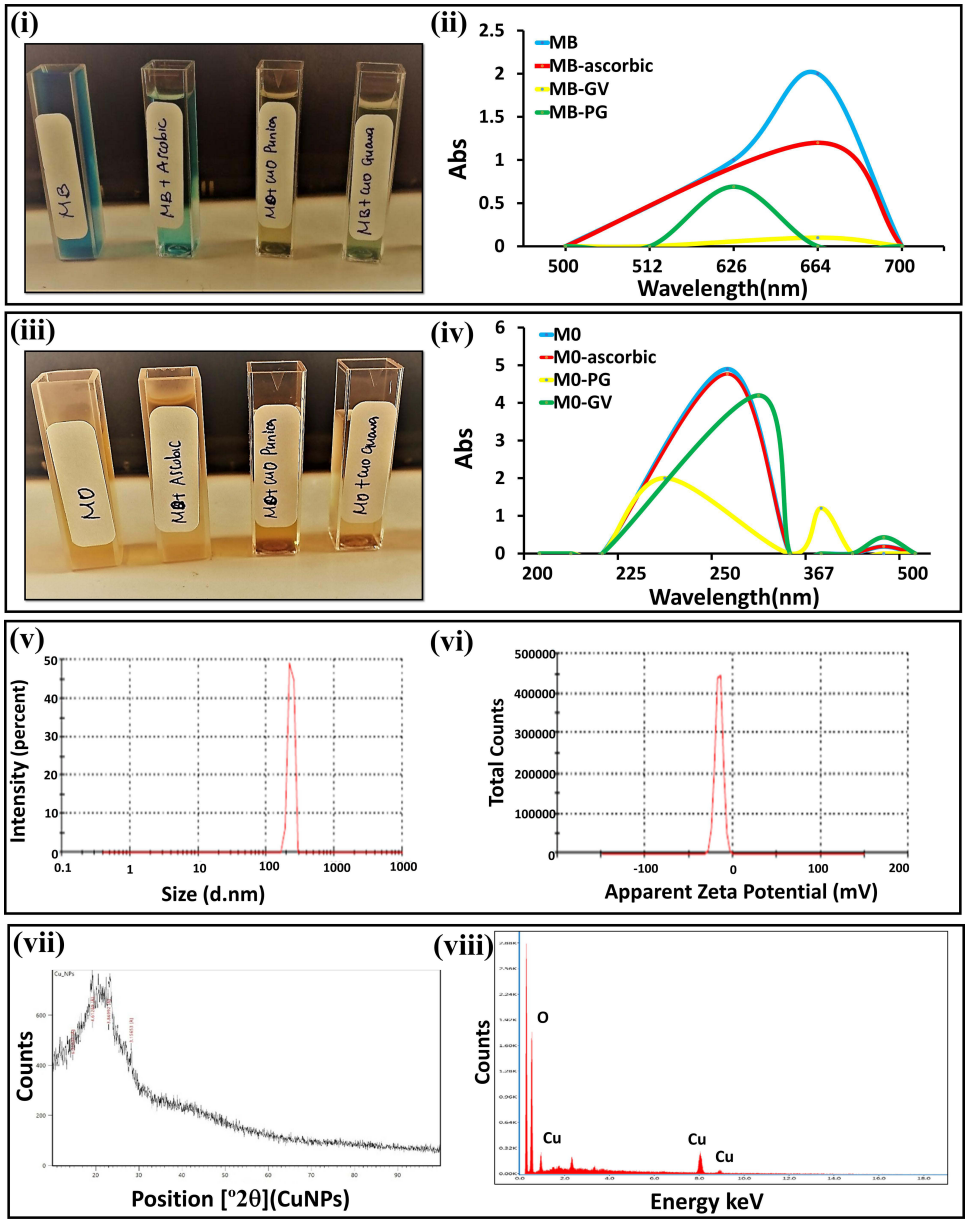

Figure 3 (**i**) Color change due to the photocatalytic degradation of MB dye in presence of CuO NPs, and (**ii**) UV-Visible absorption spectra of MB in presence and absence of CuO NPs. (**iii**) Color change due to the photocatalytic degradation of MO dye in presence of CuO NPs, and (**iv**) UV-Visible absorption spectra of MO in presence and absence of CuO NPs. (**v**) DLS measurement of particle size distribution, (**vi**) DLS measurement of zeta potential of PG-mediated CuO NPs, (**vii**) XRD pattern, and (**viii**) EDX spectra of PG-mediated CuO NPs.

any distinct zones of inhibition, as shown in Figure 4i and Table 2. According to the results, the zone of inhibition would expand if the concentration of CuO NPs were increased. Generally, the tested gram-negative bacteria group had produced the largest zones of inhibition recorded against *Escherichia coli* (34.67±2.3 mm) and *Shigella spp*. (29.3±2.52 mm) at 200µg/mL. Furthermore, CuO NPs at 250µg/mL produced a significant zone of inhibition against *Salmonella paratyphi* (29.24±3.6mm). The maximum zones of inhibition in the gram-positive bacteria group were recorded in the cases of *Staphylococcus aureus* (9.6±0.21mm), and *Staphylococcus epidermidis* (9.07±0.26mm) at 250 and 200µg/mL of CuO NPs, respectively. Moreover, the lowest inhibition zones were found at 100 and 200µg/mL against *Streptococcus spp*. (7.54±0.1mm), and *Bacillus cereus* (7.1±0.15mm), respectively. Our survey indicated that gram-negative bacteria were more effectively combated by the fabricated CuO NPs than gram-positive bacteria. The tested CuO NPs can easily break

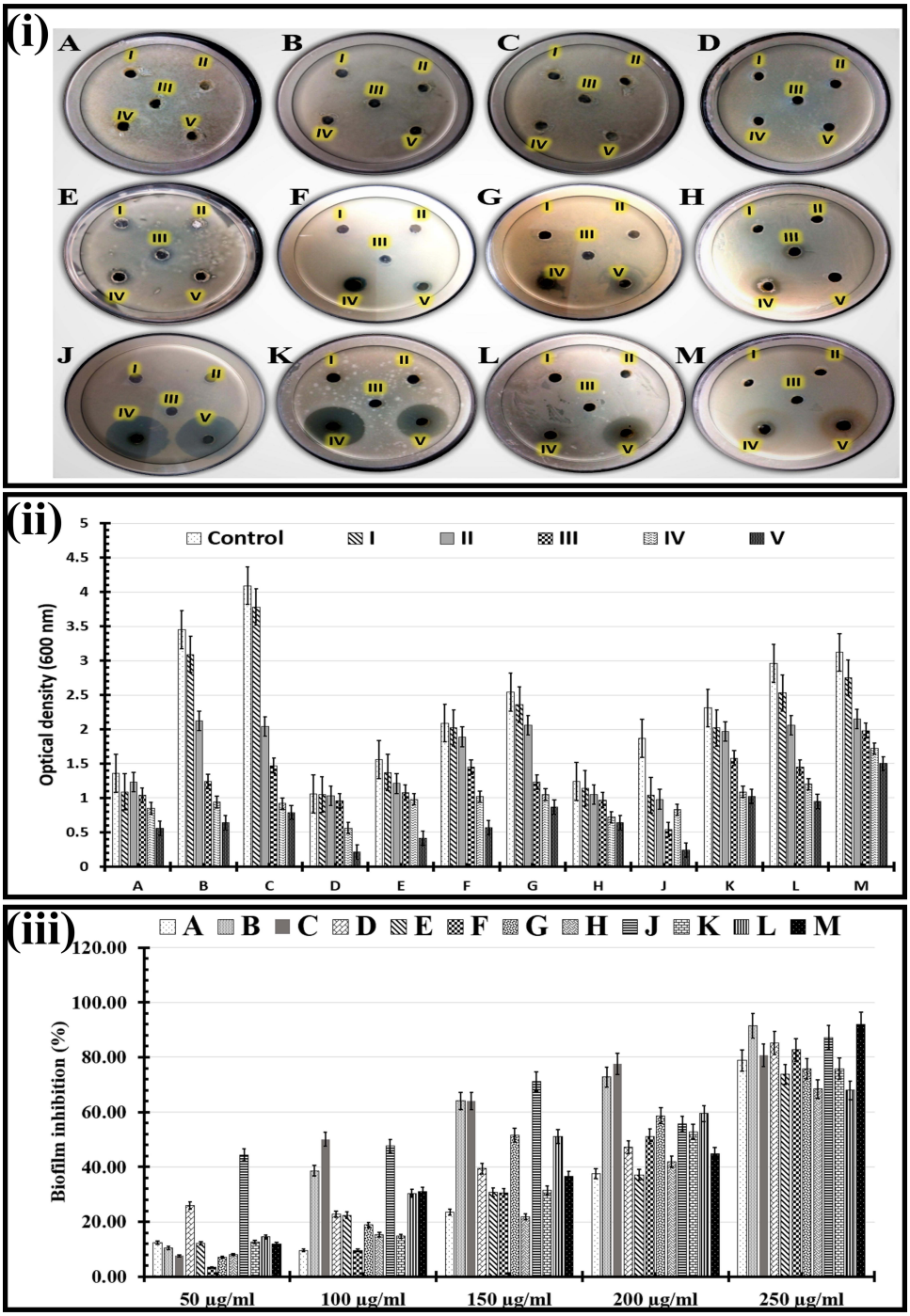

Figure 4 (**i**) Photos shown the antimicrobial activity of various CuO NPs doses; (I): 50 µg/mL, (II): 100 µg/mL, (III): 150 µg/mL, (IV): 200 µg/mL, and (V): 250 µg/mL, using Multidrug-resistant human pathogens such as (A): *Candida krusei*, (B): *Candida tropicalis*, (C): *Candida glabrata*, (D): *Candida albicans*, (E): *Streptococcus spp*., (F): *Staphylococcus epidermidis*, (G): *Staphylococcus aureus*, (H): *Bacillus cereus*, (J): *Salmonella paratyphi*, (K): *Shigella spp*, (L): *Pseudomonas aeruginosa*, and (M): *Escherichia coli*, (**ii**) Antimicrobial efficacy of different doses of CuO NPs (I): 50 µg/mL, (II): 100 µg/mL, (III): 150 µg/mL, (IV): 200 µg/mL, and (V): 250 µg/mL, using micro-dilution method against multi-drug resistant human pathogens such as (A): *Candida krusei*, (B): *Candida tropicalis*, (C): *Candida glabrata*, (D): *Candida albicans*, (E): *Streptococcus spp*., (F): *Staphylococcus epidermidis*, (G): *Staphylococcus aureus*, (H): *Bacillus cereus*, (J): *Salmonella paratyphi*, (K): *Shigella spp*, (L): *Pseudomonas aeruginosa*, and (M): *Escherichia coli*. The error bars represent the standard error of two different, triplicate studies, and (**iii**) In Vitro anti-biofilm efficacy of different dosages of CuO NPs (50, 100, 150, 200, and 250µg/mL) using Multidrug-resistant human pathogens such as (A): *Candida krusei*, (B): *Candida tropicalis*, (C): *Candida glabrata*, (D): *Candida albicans*, (E): *Streptococcus spp*., (F): *Staphylococcus epidermidis*, (G): *Staphylococcus aureus*, (H): *Bacillus cereus*, (J): *Salmonella paratyphi*, (K): *Shigella spp*, (L): *Pseudomonas aeruginosa*, and (M): *Escherichia coli*. The error bars represent the standard error of two different, triplicate studies.

Table 2 Antimicrobial Activities of Various Doses of CuO NPs That Indicated as Growth-Inhibition Zones Against Different Multidrug-Resistant Human Pathogens

Multidrug-Resistant Human Pathogens	Zone of Inhibition (mm±SD)				
	50 µg/mL	100 µg/mL	150 µg/mL	200 µg/mL	250 µg/mL
Candida krusei	0.00±0.00	0.00±0.00	0.00±0.00	0.00±0.00	0.00±0.00
Candida tropicalis	0.00±0.00	0.00±0.00	0.00±0.00	0.00±0.00	0.00±0.00
Candida glabrata	0.00±0.00	0.00±0.00	0.00±0.00	0.00±0.00	0.00±0.00
Candida albicans	0.00±0.00	0.00±0.00	0.00±0.00	0.00±0.00	0.00±0.00
Streptococcus spp.	4.21±0.10	7.54±0.10	4.74±0.15	1.67±1.53	0.00±0.00
Staphylococcus epidermidis	0.00±0.00	0.00±0.00	0.00±0.00	9.07±0.26	3.14±0.10
Staphylococcus aureus	0.00±0.00	0.00±0.00	0.00±0.00	5.01±0.25	9.6±0.21
Bacillus cereus	0.00±0.00	0.00±0.00	2.05±0.10	7.10±0.15	0.00±0.00
Salmonella paratyphi	0.00±0.00	0.00±0.00	0.00±0.00	22.67±2.60	29.24±3.60
Shigella spp	0.00±0.00	0.00±0.00	0.00±0.00	29.3±2.52	18.42±1.64
Pseudomonas aeruginosa	0.00±0.00	0.00±0.00	0.00±0.00	0.00±0.00	14.9±2.29
Escherichia coli	0.00±0.00	0.00±0.00	0.00±0.00	34.67±2.30	29.89±3.60

through the gram-negative bacteria's cell membrane and kill them because gram-positive bacteria are more likely to have thicker cell walls than gram-negative bacteria.[46]

Micro-dilution analysis has also been used to investigate CuO NP's antimicrobial effects against all tested pathogens (Figure 4ii and Table 3). This assay's high sensitivity and efficiency to distinguish between both biostatic and biocidal

Table 3 Antimicrobial Efficacy of Different Doses of CuO NPs as Well as MIC, MBC, and MFC Values Using Micro-Dilution Method Against Multidrug-Resistant Human Pathogens

Multidrug-Resistant Human Pathogens	Optical Density (600 nm ±SD)						MIC (µg/mL)	MBC (µg/mL)	MFC (µg/mL)
	Control	50 µg/mL	100 µg/mL	150 µg/mL	200 µg/mL	250 µg/mL			
Candida krusei	1.36±0.23^{a}	1.19±0.25^{a}	1.23±0.12^{ab}	1.04±0.45^{bc}	0.85±0.45^{bc}	0.56±0.09^{c}	300		400
Candida tropicalis	3.45±0.94^{a}	3.09±1.38^{a}	2.12±0.67^{ab}	1.24±0.24^{bc}	0.94±0.14^{bc}	0.64±0.07^{c}	450		500
Candida glabrata	4.09±0.19^{a}	3.78±2.12^{a}	2.04±0.45^{ab}	1.47±0.47^{bc}	0.92±0.09^{bc}	0.79±0.01^{c}	300		400
Candida albicans	1.06±0.81^{a}	1.05±0.12^{a}	1.03±0.87^{ab}	0.96±0.28^{bc}	0.56±0.07^{bc}	0.21±0.45^{c}	350		500
Streptococcus spp.	1.56±0.54^{a}	1.37±0.37^{a}	1.21±0.47^{ab}	1.08±0.27^{bc}	0.98±0.01^{bc}	0.41±0.78^{c}	300	450	
Staphylococcus epidermidis	2.09±0.18^{a}	2.02±0.89^{a}	1.89±0.14^{ab}	1.45±0.72^{bc}	1.02±0.09^{bc}	0.57±0.34^{c}	350	450	
Staphylococcus aureus	2.54±0.24^{a}	2.36±0.19^{a}	2.06±0.49^{ab}	1.23±0.48^{bc}	1.05±0.09^{bc}	0.87±0.19^{c}	400	450	
Bacillus cereus	1.24±0.48^{a}	1.14±0.14^{a}	1.05±0.37^{ab}	0.97±0.91^{bc}	0.72±0.07^{bc}	0.64±0.18^{c}	300	400	
Salmonella paratyphi	1.87±0.78^{a}	1.04±0.45^{a}	0.98±0.71^{ab}	0.54±0.05^{bc}	0.23±0.04^{bc}	0.08±0.09^{c}	250	350	
Shigella spp	2.31±0.15^{a}	2.02±0.87^{a}	1.97±0.73^{ab}	0.58±0.07^{bc}	0.09±0.12^{bc}	0.02±0.01^{c}	250	350	
Pseudomonas aeruginosa	2.96±0.89^{a}	2.53±0.97^{a}	2.06±1.09^{ab}	1.45±0.09^{bc}	0.52±0.97^{bc}	0.05±0.04^{c}	300	400	
Escherichia coli	3.12±1.56^{a}	2.75±1.07^{a}	0.15±0.97^{ab}	0.08±0.79^{bc}	0.05±0.92^{bc}	0.02±0.97^{c}	300	450	

Notes: Lowercase letters indicate significant differences between the optical densities. Similar letters indicate that there is no significant difference ^{abc}($P > 0.05$).

effects are two advantages for microbiological assay detection.[28] The produced microbial cells were detected by measuring their optical density at 600 nm. Our results showed that all tested pathogens (fungal cells, gram-negative and gram-positive bacteria) were sensitive to all used CuO NPs concentrations.

In the case of fungal cells, *Candida albicans* (0.21±0.45), *Candida krusei* (0.56±0.09), *Candida tropicalis* (0.64±0.07) followed by *Candida glabrata* (0.79±0.01) were more sensitive to CuO NPs at 250µg/mL. Additionally, the MIC values for *Candida krusei* and *Candida glabrata* were 300µg/mL. In contrast, the MIC values for *Candida albicans* and *Candida tropicalis* were 350µg/mL and 450µg/mL, respectively (Table 3). The CuO NPs' MFC is the lowest concentration of CuO NPs necessary to fully destroy fungal cells (showing no turbidity). Our results demonstrated that the CuO NPs' MFC values ranged between 400 and 500µg/mL after 24hs. The CuO NPs' MFC that could eliminate more than 99% of both *Candida krusei* and *Candida glabrata* was 400µg/mL. On the other hand, the CuO NPs' MFC that had a similar effect on *Candida tropicalis* and *Candida albicans* was tabulated to be 500µg/mL.

Additionally, the turbidity readings for gram-positive bacteria were arranged ascendingly as follows: *Streptococcus spp*. (0.41 ±0.78), *Staphylococcus epidermidis* (0.57±0.34) followed by *Bacillus cereus* (0.64±0.18) and *Staphylococcus aureus* (0.87±0.19) reported at 250µg/mL of CuO NPs. Meanwhile, the observed CuO NPs' MIC value for *Streptococcus spp*. and *Bacillus cereus* was 300µg/mL. The obtained CuO NPs' MICs for *Staphylococcus epidermidis* and *Staphylococcus aureus* were 350 and 400µg/mL, respectively. Despite *Streptococcus spp., Staphylococcus epidermidis*, and *Staphylococcus aureus* having CuO NPs' MBCs of 450µg/mL each, *Bacillus cereus* had a reported CuO NPs' MBC at 400µg/mL. All the studied gram-negative bacteria responded favorably to a dosage of 250µg/mL CuO NPs. The MBC for CuO NPs was 350µg/mL, while the recorded CuO NPs' MIC for *Shigella spp*. and *Salmonella paratyphi* were 250µg/mL. Additionally, the CuO NPs' MIC for *Escherichia coli* and *Pseudomonas aeruginosa* were 300µg/mL. On the other hand, the CuO NPs' MBCs for *Escherichia coli* and *Pseudomonas aeruginosa* were measured to be 400 and 450µg/mL, respectively.

After 18 h, the impact of various CuO NP dosages on the generation of microbial biofilms was examined and evaluated (Figure 4iii). As demonstrated in Table 4, all the investigated pathogens showed significant inhibitory effects of the biofilms. High CuO NPs dosages significantly boosted (p-value <0.05) the % of biofilm inhibitory efficacy. The maximum anti-biofilm efficacy was found at 250µg/mL CuO NPs against *Escherichia coli* (91.92±8.29), *Candida*

Table 4 Anti-Biofilm Efficacy of Different Dosages of CuO NPs Against Different Multidrug-Resistant Human Pathogens in-vitro

Multidrug-Resistant human pathogens	Biofilm Inhibition (%±SD)				
	50 µg/mL	100 µg/mL	150 µg/mL	200 µg/mL	250 µg/mL
Candida krusei	12.5±6.23^{c}	9.56±2.36^{c}	23.53±17.36^{b}	37.5±5.23^{b}	78.82±1.28^{a}
Candida tropicalis	10.43±1.78^{c}	38.55±8.33^{c}	64.06±4.12^{b}	72.75±3.69^{b}	91.45±4.69^{a}
Candida glabrata	7.58±3.59^{c}	50.12±8.12^{c}	64.06±3.56^{b}	77.51±5.09^{b}	80.68±6.45^{a}
Candida albicans	25.94±10.36^{c}	22.83±14.23^{c}	39.43±6.23^{b}	47.17±8.12^{b}	85.19±9.12^{a}
Streptococcus spp.	12.18±4.78^{c}	22.44±8.12^{c}	30.77±7.15^{b}	37.18±0.78^{b}	73.72±9.17^{a}
Staphylococcus epidermidis	3.35±1.09^{c}	9.57±4.12^{c}	30.62±8.12^{b}	51.19±8.94^{b}	82.73±14.23^{a}
Staphylococcus aureus	7.09±2.07^{c}	18.89±3.69^{c}	51.57±4.78^{b}	58.66±7.56^{b}	75.75±9.14^{a}
Bacillus cereus	8.06±6.82^{c}	15.32±1.85^{c}	21.77±0.78^{b}	41.94±15.36^{b}	68.39±9.18^{a}
Salmonella paratyphi	44.39±7.89^{c}	47.59±11.23^{c}	71.12±17.36^{b}	75.61±9.45^{b}	87.17±18.36^{a}
Shigella spp.	12.55±12.83^{c}	14.71±9.38^{c}	31.60±9.78^{b}	52.81±7.52^{b}	75.84±10.26^{a}
Pseudomonas aeruginosa	14.53±5.48^{c}	30.41±9.07^{c}	51.01±10.24^{b}	59.46±8.04^{b}	67.91±11.05^{a}
Escherichia coli	11.86±9.03^{c}	31.09±9.36^{c}	36.54±8.94^{b}	44.87±3.05^{b}	91.92±8.29^{a}

Notes: Lowercase letters indicate significant differences between the biofilms formed. Similar letters indicate that there is no significant difference ^{abc}($P > 0.05$).

tropicalis (91.45±4.69%), and *Salmonella paratyphi* (87.17±18.36%). Additionally, the results showed that *Candida albicans* (85.19±9.12%) and *Staphylococcus epidermidis* (82.73±14.23%) were more responsive to the 250µg/mL of CuO NPs than *Bacillus cereus* (68.39±9.18%) and *Pseudomonas aeruginosa* (67.91±11.05%). By checking developed colonies in all investigated specimens, the MBIC, or the lowest concentration of CuO NPs required to prevent biofilm growth, was discovered to be greater than 250µg/mL.

The primary factor affecting CuO NPs' ability to suppress biofilm is the size of their particulates, as smaller particles have a higher surface area for interacting with pathogens.[29] By rupturing microbial cell wall or cell membrane, copper ions can inhibit the growth and development of pathogens. Inside the cell, nanoparticles will interact with phosphorus- and sulphur-rich molecules like DNA, as well as microbial enzymes.[47] Additionally, copper ions produced from CuO NPs were associated with anti-biofilm effects due to their ability to completely cover pathogen surfaces and destroy them via modifying the performance of proteins and enzymes.[48] Depending on the physiochemical characteristics of the broth culture, CuO NPs considerably limit biofilm growth and reduce cellular enzyme activity, which inhibits cell permeability.[49]

Ex-Vivo Cell Line Studies

Determination of Cytotoxicity of CuO NPs on Normal Skin Cells

Tailored green synthesized CuO NPs cytotoxic potential was evaluated against HBF4 with various concentrations ranging from 0.1% to 08% w/v. Results revealed a dose-dependent cytotoxicity, where lower a CuO NPs concentration (1 mg/mL) showed 94.10±0.42% viability, and this viability was declined to 72.82±1.19% at a higher concentration of 8mg/mL. IC_{50} of CuO NPs against HBF4 cells was found to be 1.002±0.05%. Meanwhile, EC_{100} was 0.071±0.001% as shown in Figure 5i. This may be attributed to the role reported by Sankar et al[50] that CuO NPs can cause numerous morphological modifications on tested cells including alteration in cells' shape and inhibition of cell communications. Subsequently, a prompt cell apoptosis pathway via the production of reactive oxygen species would occur. Based on the EC_{100} values, 0.2% w/v was selected to investigate the wound healing efficacy of CuO NPs.[50]

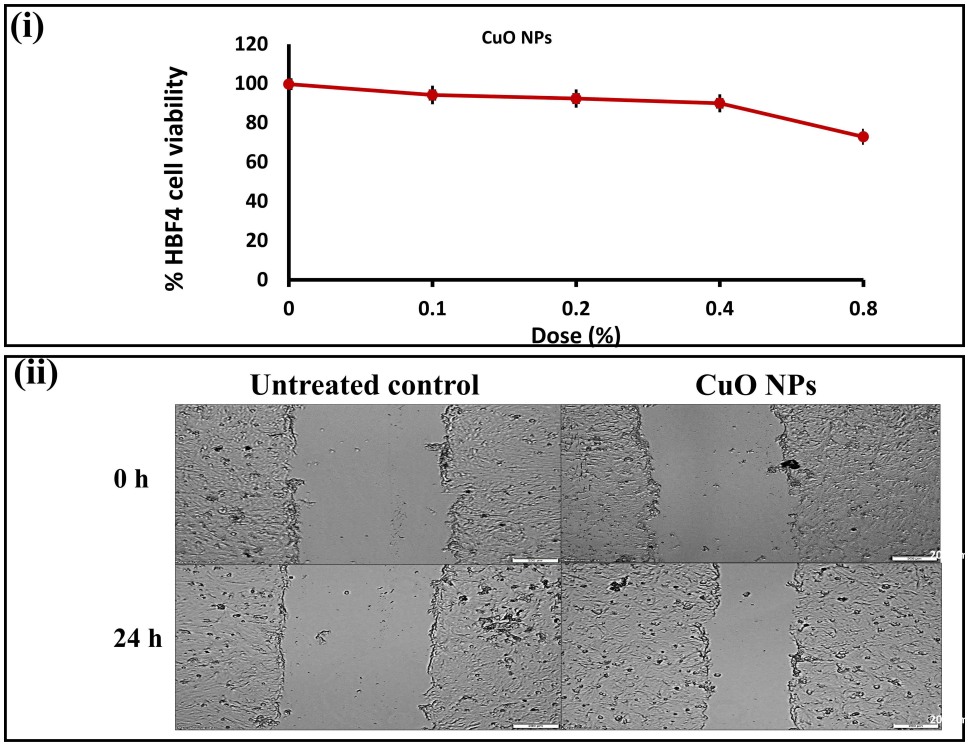

Figure 5 (**i**) The % of HBF4 cell viability after incubation for 24 h in 5% CO_2 with different concentrations of CuO NPs (0–0.8% w/v), and (**ii**) Microscopic images of wound area in the untreated control HBF4 cells and after 24 h treatment with free CuO NPs.

Wound Scratch Healing Assay

A wound scratch assay was conducted to estimate the proliferation patterns, as well as the migration of HBF4 fibroblasts in response to the application of CuO NPs. Fibroblasts must proliferate and then migrate to the wound bed to induce effective healing and tissue regeneration of the wound. Owing to their role in the secretion of the extracellular matrix collagen of the granulation tissue, neo-angiogenesis can start up.[34] Compared to the control, the wells treated with CuO NPs significantly exhibited 29.460±0.811% healing of the scratched wound compared to 2.001±0.155% for the untreated wounds (Figure 5ii). This can be explained by the participation of copper itself in the process of angiogenesis. Copper initiates extracellular matrix skin proteins' synthesis and stabilization. Moreover, the expression of inducible vascular endothelial growth factor, which has a crucial role in angiogenesis process, is sensitive to copper.[20,51] As a result, an acceleration of dermal wound contraction and closure was observed.

In-Vivo Wound Healing Activity

Wound Healing Assessment

The complication of wound healing in diabetic wound environment is the major factor impairing the healing activity. For instance, copper, a key element playing a vital role in wound healing by inducing angiogenesis with a bactericidal effect, is proven to have imbalanced levels in diabetic patients.[52]

The application of copper salts or oxides is thought to be convenient; however, their toxicity is always raising a concern.[8] In this regard, for estimating the wound healing ability of the CuO NPs, two concentrations of CuO NPs powder (2mg and 10 mg/cm^2) were tested on exposed rats' wounds. Mean wound contraction rates were calculated. Photographs of the wound repair process at intervals are displayed in Figure 6i. The wound areas were observed at determined time intervals. Table 5 shows the reduction in wound area as calculated. There was no rat mortality throughout the post-operative period until scarification. WC_{50} values of CuO powder were lower than those observed in the control group (11.7 days). Gp 2 treated with 2 mg/cm^2 exhibited a lower WC_{50} of 7.2 days and about 92% of wound contraction after 13 days. On the contrary, wounds treated with 10 mg/cm^2 showed only 65% of wound contraction. Gp 2, CuO NPs-treated, wounds showed the absence of any evidence of pus formation, bleeding, or any form of microbial contamination at any point of treatment, whereas control wound and wound treated with a high concentration of CuO NPs (Gp 1) showed a notable inflammation (Figure 6i).

The CuO NPs-treated group at a concentration of 2 mg/cm^2 (Gp 2) distinguished higher wound closure rates throughout all treatment days as compared with the control group. A possible explanation is that CuO NPs strongly arrested the bacterial strains found in the wound bed, leading to the proper restoration of the tissue integrity and thus, a satisfactory repair of damaged sites.[53] Moreover, CuO NPs provided a source of copper ions that may have enhanced collagen fibers and fibroblast activation, promoting tissue regeneration of the wound.[20,54] The wound toxicity at the end of the study observed in Gp 1 upon using a higher concentration of CuO NPs can be referred to as the accumulation of CuO NPs on the wound.

Normally, copper ions are readily metabolized by our bodies when absorbed orally or topically and excess copper can be readily secreted via feces and urine. In diabetic wounds, a low blood supply is provided to that area, which favored the danger of copper accumulation and local toxicity.[55]

Histopathological Examination (H&E, MTS)

Histological examination of all skin sections from in-vivo experiments offered an insight into the significance of each of the treatments where it assesses the epidermal re-epithelialization, skin-adnexal regeneration, phases of wound healing, the amount of inflammatory infiltrate, granulation tissue and fibrosis (Figure 6ii). Sections of wounds stained by H&E from the control group showed the improper healing process of the wound, where epidermal ulceration was covered by fibrinoid exudate entangling mixed acute and chronic inflammatory cells with extensive heavy inflammatory infiltrate at the dermis and subcutaneous tissue. MTS revealed minimal staining with an increased number of myofibroblasts and newly formed blood vessels as well as an increased number of lymphocytes. The wound sections from Gp 1 treated with CuO NPs (10 mg/cm^2) illustrated an obvious inflammatory phase of the healing process where the sections showed residual epidermal ulceration with extensive inflammation and granulation tissue. The sections also illustrated mild

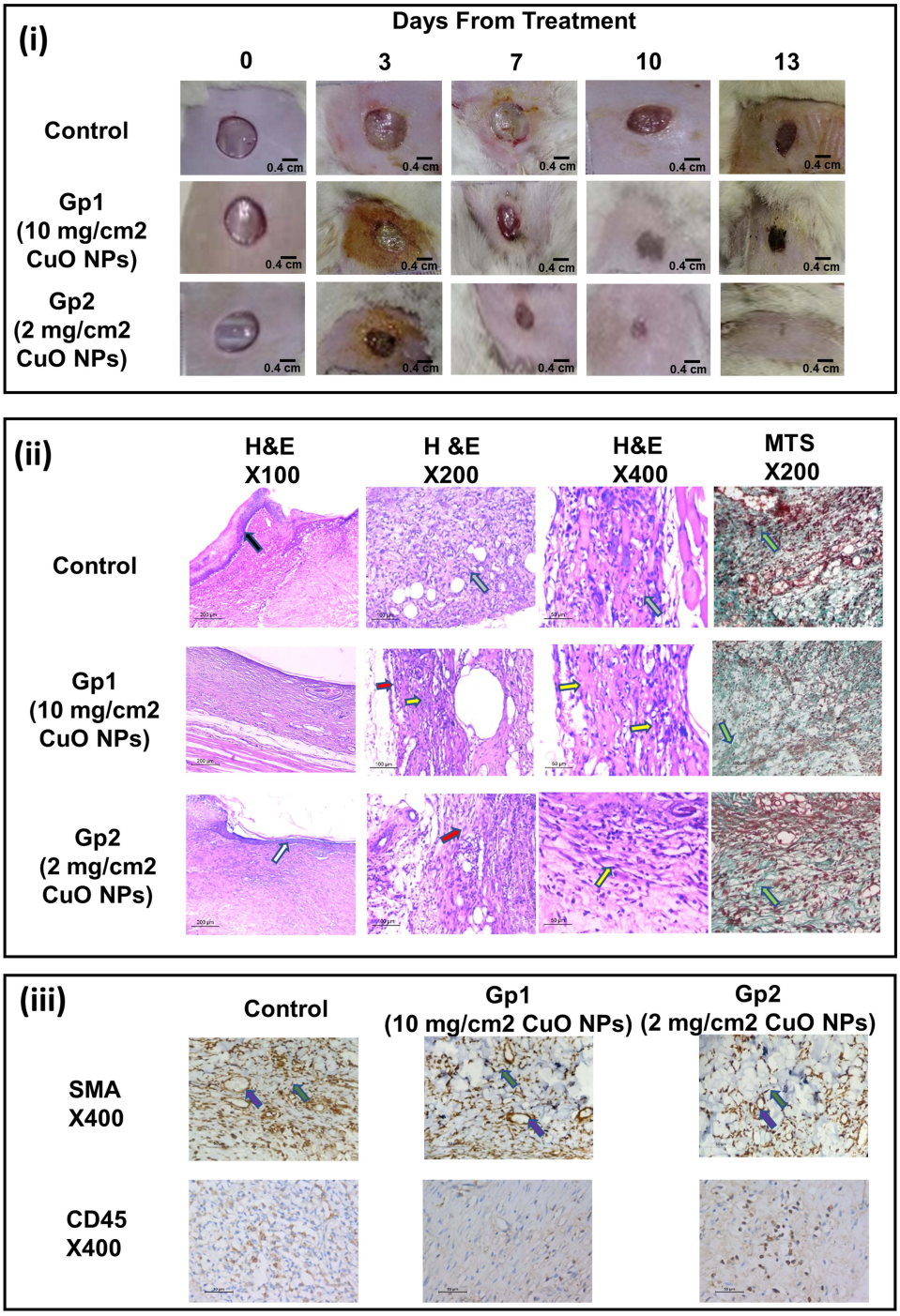

Figure 6 (**i**) Photographic images of in-vivo excision wound area contraction rate vs day of observation using dorsal of rats, (**ii**) Histological examination of H&E and MTS-stained sections of wounds, and (**iii**) Immunohistochemical (IHC) staining of excised skin sections using SMA and CD45.

fibrosis with an increased amount of the present inflammatory cells. Moreover, MTS revealed mild fibrosis, and IHC highlights the myofibroblasts and newly formed blood vessels as well as the lymphocytes. On the contrary, the wound sections from Gp 2 treated with CuO NPs (2 mg/cm^2) depicted a transition between inflammatory and remodeling phases of healing showing thin epidermal epithelialization with absent skin adnexa regeneration and little fibrous tissue deposition. It also showed a large amount of granulation tissue. Moderate fibrosis and newly formed blood vessels as

Table 5 Effect of the Application of Different Concentrations of CuO NPs Powder on Excision Wound Area Contraction and Half Closure Time (Values are Mean±SD, n=6 Observations in Each Group)

Day	Wound Contraction (%)		
	Control	Gp1 CuO NPs (10 mg/cm^2)	Gp2 CuO NPs (2 mg/cm^2)
3	7.3±0.15	10.1±2.6	18.9±3.1
7	10.2±1.7	30.5±1.9	48.5±2.4
10	35.4±2.1	45.1±2.8	78.2±1.9
13	62.3±1.8	65.0±2.4	92.1±2.1
*WC_{50} (day)	11.7	10.6	7.2

Note: Values are significant (#) at $P < 0.05$ as compared to the untreated group (control).
Abbreviation: *WC_{50}, half closure time of wound contraction in days.

well as lymphocytes were also observed after MTS. This further confirmed the superiority of 2 mg/cm^2 CuO NPs-treated group.

Immunohistochemical (IHC) Staining and Interpretation

CD45 and α-SMA were used to stain the lymphocytes, blood vessels, and myofibroblasts, respectively, as shown in Figure 6iii. Skin specimen from untreated control group exhibited massive epidermal ulceration and crust formation of 43 ±1.9, lacking skin appendages. The dermis was in the inflammatory phase with a minimal amount of fibrous tissue of 1.2 ±0.7/HPF. The neovascularization was 32±2.4/HPF, myofibroblasts 43±3.1/HPF, and lymphocytes 82±2.6/HPF. Gp 1 treated with CuO NPs (10 mg/cm^2) demonstrated the inflammatory healing phase formed of few amounts of fibrous tissue 6.8±4.7/HPF, an increased granulation tissue originated from novel developed blood vessels 66±1.8/HPF, myofibroblasts 48±8.3/HPF, and the number of lymphocytes 64±2.8/HPF. Gp 2 treated with CuO NPs (2 mg/cm^2) demonstrated the inflammatory healing phase formed of small amounts of fibrous tissue 5.7±3.7/HPF, an increased granulation tissue made up of newly formed blood vessels 70±1.5/HPF, myofibroblasts 53±2.6/HPF, and the number of lymphocytes 70±3.1/HPF. The histological and immunobiological outcomes confirmed the obtained in-vivo results.

Conclusions

Green synthesis of metal oxide NPs is an inexpensive, safe, eco-friendly, and convenient method approaching CuO synthesis. In the current research work, our team conducted a comparative study on the extracts of two different plants grown in Egypt, for the first time, to explore their reducing efficiency for CuO NPs synthesis process and their effect on the physicochemical characteristics and yield of the obtained NPs. PG peels and GV extracts were elected as suitable plant candidates for the process, where further investigation proved the superiority of PG extract synthesized CuO NPs in terms of obtained yield and photocatalytic activity. The tailored CuO NPs exhibited a spherical shape within an accepted nanometric size of 233 nm. CuO NPs synthesis was confirmed via FT-IR, UV–vis spectroscopy, TEM, SEM, XRD, and EDX studies. CuO NPs doses demonstrated strong biocidal effectiveness against all tested pathogens in the conducted antimicrobial bioassays. The wound scratch experiment showed that CuO NPs significantly exhibited 29.460±0.811% healing of the scratched wound compared to 2.001±0.155% for the untreated wound. Wound healing experiments revealed the safety of low CuO NPs concentration in a diabetic animal model as well as on a human normal skin fibroblast cell line. The treated group with a dose of 2 mg/cm^2 showed enhanced tissue regeneration compared to the control untreated and 10 mg/cm^2-treated wounds in terms of local effects and wound contraction rates. The obtained results were further confirmed by histopathological and immunohistochemical investigations. The fabricated CuO NPs can be considered suitable candidates to be further loaded in pharmaceutical polymeric films or nanofibers for tissue regeneration and wound healing purposes in diabetics.

Ethical Conduct of Research

The authors state that they have followed the principles outlined in the Declaration of Helsinki for all animal experimental investigations.

Disclosure

The authors report no conflicts of interest in this work. The authors have no relevant affiliations or financial involvement with any organization or entity with a financial interest, financial conflict with the subject matter or materials discussed in the manuscript. This includes employment, consultancies, honoraria, stock ownership or options, expert testimony, grants or patents received or pending, or royalties. No writing assistance was utilized in the production of this manuscript.

References

1. Calabrese V, Cornelius C, Dinkova-Kostova AT, Calabrese EJ, Mattson MP. Cellular stress responses, the hormesis paradigm, and vitagenes: novel targets for therapeutic intervention in neurodegenerative disorders. *Antioxid Redox Signal*. 2010;13(11):1763–1811. doi:10.1089/ars.2009.3074
2. Calabrese V, Mancuso C, Calvani M, Rizzarelli E, Butterfield DA, Giuffrida Stella AM. Nitric oxide in the central nervous system: neuroprotection versus neurotoxicity. *Nat Rev Neurosci*. 2007;8(10):766–775. doi:10.1038/nrn2214
3. Calabrese V, Guagliano E, Sapienza M, Mancuso C, Butterfield DA, Stella A. Redox regulation of cellular stress response in neurodegenerative disorders. *Ital J Biochem*. 2006;55(3–4):263–282.
4. Ma L, Gao C, Mao Z, et al. Collagen/chitosan porous scaffolds with improved biostability for skin tissue engineering. *Biomaterials*. 2003;24 (26):4833–4841. doi:10.1016/S0142-9612(03)00374-0
5. El-Lakany SA, Kamoun EA, Abd-Elhamid AI, Aly RG, Samy WM, Elgindy NA. Graphene oxide crosslinked-zein nanofibrous scaffolds for prominent Cu-adsorption as tissue regeneration promoters in diabetic rats: nanofibers optimization and in vivo assessment. *Int J Pharm*. 2020;590:119919. doi:10.1016/j.ijpharm.2020.119919
6. Qamar H, Rehman S, Chauhan DK, Tiwari AK, Upmanyu VJ. Green synthesis, characterization and antimicrobial activity of copper oxide nanomaterial derived from Momordica charantia. *Int J Nanomed*. 2020;15(2541):2541–2553. doi:10.2147/IJN.S240232
7. Javadhesari SM, Alipour S, Mohammadnejad S, Akbarpour MJMS. Antibacterial activity of ultra-small copper oxide (II) nanoparticles synthesized by mechanochemical processing against S. aureus and E. coli. *Mater Sci Eng C Mater Biol Appl*. 2019;105:110011. doi:10.1016/j.msec.2019.110011
8. Sankar R, Baskaran A, Shivashangari KS, Ravikumar VJ. Inhibition of pathogenic bacterial growth on excision wound by green synthesized copper oxide nanoparticles leads to accelerated wound healing activity in Wistar Albino rats. *J Mater Sci*. 2015;26(7):1–7.
9. Padma PN, Kumari SC, Banu ST. Effect of diverse factors on green synthesis of copper nanoparticles. *Int J Life Sci*. 2018;6:659–664.
10. Akintelu SA, Folorunso AS, Folorunso FA, Oyebamiji AKJH. Green synthesis of copper oxide nanoparticles for biomedical application and environmental remediation. *Heliyon*. 2020;6(7):e04508. doi:10.1016/j.heliyon.2020.e04508
11. Sathiyavimal S, Vasantharaj S, Veeramani V, et al. Green chemistry route of biosynthesized copper oxide nanoparticles using Psidium guajava leaf extract and their antibacterial activity and effective removal of industrial dyes. *J Environ Chem Eng*. 2021;9(2):105033.
12. Nasrollahzadeh M, Sajadi SM, Maham MJRA. Tamarix gallica leaf extract mediated novel route for green synthesis of CuO nanoparticles and their application for N-arylation of nitrogen-containing heterocycles under ligand-free conditions. *RSC Adv*. 2015;5(51):40628–40635.
13. Velsankar K, Preethi RM, Muthulakshmi V, Sudhahar SJ. Green synthesis of CuO nanoparticles via Allium sativum extract and its characterizations on antimicrobial, antioxidant, antilarvicidal activities. J Environ Chem Eng. 2020;8(5):104123.
14. Vishveshvar K, Krishnan A, Haribabu K, Vishnuprasad SJB. Green synthesis of copper oxide nanoparticles using Ixiro coccinea plant leaves and its characterization. *BioNanoScience*. 2018;8(2):554–558.
15. Yugandhar P, Vasavi T, Jayavardhana Rao Y, Uma Maheswari Devi P, Narasimha G, Savithramma NJ. Cost effective, green synthesis of copper oxide nanoparticles using fruit extract of Syzygium alternifolium (Wt.) Walp., characterization and evaluation of antiviral activity. *J Clust Sci*. 2018;29(4):743–755.
16. Das P, Ghosh S, Ghosh R, Dam S, Baskey MJ, Biology PB. Madhuca longifolia plant mediated green synthesis of cupric oxide nanoparticles: a promising environmentally sustainable material for waste water treatment and efficient antibacterial agent. *J Photochem Photobiol B Biol*. 2018;189:66–73. doi:10.1016/j.jphotobiol.2018.09.023
17. Rabiee N, Bagherzadeh M, Kiani M, et al. Biosynthesis of copper oxide nanoparticles with potential biomedical applications. *Int J Nanomed*. 2020;15:3983. doi:10.2147/IJN.S255398
18. Shammout M, Awwad AJMS. A novel route for the synthesis of copper oxide nanoparticles using Bougainvillea plant flowers extract and antifungal activity evaluation. *Chem Int*. 2021;7(1):71–78.
19. Nagajyothi P, Muthuraman P, Sreekanth T, Kim DH, Shim JJA. Green synthesis: in-vitro anticancer activity of copper oxide nanoparticles against human cervical carcinoma cells. *Arab J Chem*. 2017;10(2):215–225.
20. Borkow G, Gabbay J, Dardik R, et al. Molecular mechanisms of enhanced wound healing by copper oxide-impregnated dressings. *Wound Repair Regen*. 2010;18(2):266–275. doi:10.1111/j.1524-475X.2010.00573.x
21. Shi L-B, Tang P-F, Zhang W, Zhao Y-P, Zhang L-C, Zhang HJT. Green synthesis of CuO nanoparticles using Cassia auriculata leaf extract and in vitro evaluation of their biocompatibility with rheumatoid arthritis macrophages (RAW 264.7). *Trop J Pharm Res*. 2017;16(1):185–192.
22. Adam RE, Alnoor H, Pozina G, Liu X, Willander M, Nur OJ. Synthesis of Mg-doped ZnO NPs via a chemical low-temperature method and investigation of the efficient photocatalytic activity for the degradation of dyes under solar light. *Solid State Sci*. 2020;99:106053.
23. Aasy NKA, Ragab D, Sallam MA, Abdelmonsif DA, Aly RG, Elkhodairy KA. A comparative study: the prospective influence of nanovectors in leveraging the chemopreventive potential of COX-2 inhibitors against skin cancer. *Int J Nanomedicine*. 2019;14:7561. doi:10.2147/IJN.S218905

24. Akintelu SA, Olugbeko SC, Folorunso AS. A review on synthesis, optimization, characterization and antibacterial application of gold nanoparticles synthesized from plants. *Int Nano Lett*. 2020;10(4):237–248.
25. Hayat S, Ashraf A, Zubair M, et al. Biofabrication of ZnO nanoparticles using Acacia arabica leaf extract and their antibiofilm and antioxidant potential against foodborne pathogens. *PLoS One*. 2022;17(1):e0259190. doi:10.1371/journal.pone.0259190
26. Bukhari SI, Hamed MM, Al-Agamy MH, Gazwi HS, Radwan HH, Youssif AM. Biosynthesis of copper oxide nanoparticles using Streptomyces MHM38 and its biological applications. *J Nanomater*. 2021;2021:1–16. doi:10.1155/2021/6693302
27. Kashyap AK, Kashyap A, Deshmukh L, Vishwakarma D, Vishwakarma D. Biosynthesis and biophysical elucidation of CuO nanoparticle from Nyctanthes arbor-tristis Linn Leaf. *Appl Microbiol Biotechnol*. 2022;106(17):5823–5832. doi:10.1007/s00253-022-12105-8
28. Al-Dhabi NA, Ghilan A-KM, Arasu MV, Duraipandiyan V. Green biosynthesis of silver nanoparticles produced from marine Streptomyces sp. Al-Dhabi-89 and their potential applications against wound infection and drug resistant clinical pathogens. *J Photochem Photobiol B*. 2018;189:176–184. doi:10.1016/j.jphotobiol.2018.09.012
29. Shehabeldine AM, Amin BH, Hagras FA, et al. Potential Antimicrobial and antibiofilm properties of copper oxide nanoparticles: time-kill kinetic essay and ultrastructure of pathogenic bacterial cells. *Appl Biochem Biotechnol*. 2022;2022:1–19.
30. Youngish I, El-Hawary S, Eldahshan O, Abdel-Aziz M, Ali Z. Green synthesis of magnesium nanoparticles mediated from Rosa floribunda charisma extract and its antioxidant, antiaging and antibiofilm activities. *Sci Rep*. 2021;11:16868. doi:10.1038/s41598-021-96377-6
31. Nguyen N-YT, Grelling N, Wetteland CL, Rosario R, Liu H. Antimicrobial activities and mechanisms of magnesium oxide nanoparticles (nMgO) against pathogenic bacteria, yeasts, and biofilms. *Sci Rep*. 2018;8(1):1–23. doi:10.1038/s41598-018-34567-5
32. Clinical, Institute LS. *Performance Standards for Antimicrobial Susceptibility Testing*. PA: Clinical and Laboratory Standards Institute Wayne; 2017.
33. Krishnan BR, Ramesh M, Selvakumar M, et al. A facile green approach of cone-like ZnO NSs synthesized via jatropha gossypifolia leaves extract for photocatalytic and biological activity. *J Inorg Organomet Polym Mater*. 2020;30(11):4441–4451. doi:10.1007/s10904-020-01576-9
34. El-Lakany SA, Abd-Elhamid AI, Kamoun EA, El-Fakharany EM, Samy WM, Elgindy NA. α-Bisabolol-loaded cross-linked zein nanofibrous 3d-scaffolds for accelerating wound healing and tissue regeneration in rats. *Int J Nanomedicine*. 2019;14:8251–8270. doi:10.2147/IJN.S224315
35. You C, Li Q, Wang X, et al. Silver nanoparticle loaded collagen/chitosan scaffolds promote wound healing via regulating fibroblast migration and macrophage activation. *Sci Rep*. 2017;7(1):10489. doi:10.1038/s41598-017-10481-0
36. Samy W, Elgindy N, El-Gowelli HM. Biopolymeric nifedipine powder for acceleration of wound healing. *Int J Pharm*. 2012;422(1–2):323–331. doi:10.1016/j.ijpharm.2011.11.021
37. Rafique M, Sadaf I, Rafique MS, Tahir MB. A review on green synthesis of silver nanoparticles and their applications. *Artif Cells Nanomed Biotechnol*. 2017;45(7):1272–1291. doi:10.1080/21691401.2016.1241792
38. Thenmozhi S, Rajan S. GC-MS analysis of bioactive compounds in Psidium guajava leaves. *J Pharmacogn Phytochem*. 2015;3(5):162–166.
39. Abdel-Aziz S, El-Esawi M, Hazaa M, Abdel-Aziz HY, Hassan MG. Antibacterial potential of pomegranate peel extracts on Escherichia coli isolated from Benha hospital in Egypt. *Benha J Appl Sci*. 2021;6(3):61–64. doi:10.21608/bjas.2021.169813
40. Ealia SAM, Saravanakumar M. A review on the classification, characterisation, synthesis of nanoparticles and their application. Paper presented at: IOP conference series: materials science and engineering; 2017.
41. Reddy KR. Green synthesis, morphological and optical studies of CuO nanoparticles. *J Mol Struct*. 2017;1150:553–557.
42. Paul S, Sheyi A, Bangu ID, Abubakar SI, Muhammad MMJW. Biological synthesis and characterization of copper oxide nanoparticles using aqueous Psidium guajava leaf extract and study of antibacterial activity of the copper oxide nanoparticles on Escherichia coli and Staphylococcus aureus. *World J Adv Res Rev*. 2021;9(1):114–120.
43. Sadollahkhani A, Nur O, Willander M, et al. A detailed optical investigation of ZnO@ ZnS core–shell nanoparticles and their photocatalytic activity at different pH values. *Ceram Int*. 2015;41(5):7174–7184.
44. Nabila MI, Kannabiran KJB. Biosynthesis, characterization and antibacterial activity of copper oxide nanoparticles (CuO NPs) from actinomycetes. *Biocatal Agri Biotechnol*. 2018;15:56–62.
45. Padil VVT, Černík MJ. Green synthesis of copper oxide nanoparticles using gum karaya as a biotemplate and their antibacterial application. *Int J Nanomed*. 2013;8:889.
46. Ammulu MA, Vinay Viswanath K, Giduturi AK, Vemuri PK, Mangamuri U, Poda S. Phytoassisted synthesis of magnesium oxide nanoparticles from Pterocarpus marsupium rox. b heartwood extract and its biomedical applications. *J Genet Eng Biotechnol*. 2021;19(1):1–18. doi:10.1186/s43141-021-00119-0
47. Rajivgandhi G, Maruthupandy M, Muneeswaran T, et al. Biologically synthesized copper oxide nanoparticles enhanced intracellular damage in ciprofloxacin resistant ESBL producing bacteria. *Microb Pathog*. 2019;127:267–276. doi:10.1016/j.micpath.2018.12.017
48. Kasemets K, Ivask A, Dubourguier H-C, Kahru A. Toxicity of nanoparticles of ZnO, CuO and TiO2 to yeast Saccharomyces cerevisiae. *In Vitro Toxicol*. 2009;23(6):1116–1122. doi:10.1016/j.tiv.2009.05.015
49. Singh A, Gautam PK, Verma A, et al. Green synthesis of metallic nanoparticles as effective alternatives to treat antibiotics resistant bacterial infections: a review. *Biotechnol Rep*. 2020;25:e00427. doi:10.1016/j.btre.2020.e00427
50. Sankar R, Maheswari R, Karthik S, Shivashangari KS, Ravikumar V. Anticancer activity of Ficus religiosa engineered copper oxide nanoparticles. *Mater Sci Engineer*. 2014;44:234–239. doi:10.1016/j.msec.2014.08.030
51. Sen CK, Khanna S, Venojarvi M, et al. Copper-induced vascular endothelial growth factor expression and wound healing. *Am J Physiol Heart Circ Physiol*. 2002;282(5):H1821–H1827. doi:10.1152/ajpheart.01015.2001
52. Atari-Hajipirloo S, Valizadeh N, Khadem-Ansari M-H, Rasmi Y, Kheradmand FJ. Altered concentrations of copper, zinc, and iron are associated with increased levels of glycated hemoglobin in patients with type 2 diabetes mellitus and their first-degree relatives. *Int J Endocrinol Metab*. 2016;14(2):1.
53. Barroso A, Mestre H, Ascenso A, Simões S, Reis CJNS, Seymour H. Nanomaterials in wound healing: from material sciences to wound healing applications. *Bone Jt Open*. 2020;1(5):443–460. doi:10.1302/2633-1462.18.BJO-2020-0089.R1
54. Tiwari M, Jain P, Hariharpura RC, Udupa N, Rao JV. In vitro wound-healing effects of biosynthesized copper nanoparticles. *Asian J Pharm Sci*. 2016;11(1):158–159.
55. Borkow G, Okon-Levy N, Gabbay J. Copper oxide impregnated wound dressing: biocidal and safety studies. *Wounds*. 2010;22(12):301–310.